Measurements of the hydrogen 2s-2p coherence using the quantum-beat technique

Robert DeSerio, Carlos Gonzalez-Lepera, John P. Gibbons, Joachim Burgdörfer, and I. A. Sellin
Department of Physics, University of Tennessee, Knoxville, Tennessee 37996
and Oak Ridge National Laboratory, Oak Ridge, Tennessee 37831
(Received 5 October 1987)

We have measured Lyman-α quantum beats from coherently excited hydrogen atoms produced in 85–235-keV proton collisions with a thin helium jet target. Intensity measurements of the radiation emitted at 90° to the beam direction as a function of distance downstream from the target in electric fields both parallel and antiparallel to the beam axis allow extraction of the coherence between the s and p states by Eck's method [Phys. Rev. Lett. **31**, 270 (1973)]. Because the jet target allows the collisions to occur in the applied field, we have eliminated the problems associated with field inhomogeneities when gas target cells are used. A strong-intensity peak emitted by excited helium in the target allows a determination of the starting point of the evolution in the field as well as a determination of the effects of experimental averaging. We present the s-p coherence parameters as a function of the projectile energy and compare them with recent theoretical calculations.

INTRODUCTION

Recent theoretical and experimental investigations have begun to answer fundamental questions concerning the shape of the charge cloud formed in electron-capture processes in simple ion-atom collisions. Measurements and calculations of substate cross sections[1] for capture into different angular momentum states are being complemented by studies of the shape and circulation of the electron cloud produced in the collision.[2–6] Alignment and orientation (Zeeman coherences) describe the nonstatistical population of different $|lm\rangle$ magnetic substates in an angular momentum level l and give the quadrupole deformation and net angular momentum. Because of the l degeneracy of the Coulomb system, coherences between different angular momentum states within a principal shell are observable most conveniently in hydrogenic systems and provide information about the dipole moment and perihelion velocity.[7] Just as the Zeeman coherences can be related to expectation values of multipoles of the angular momentum operator L, angular momentum coherences can be related to expectation values of multipoles built up from L and the Runge-Lenz vector A, a second constant of the motion for the Coulomb potential. Angular momentum coherences have also recently been observed in the autoionization spectrum of doubly excited manifolds[8,9] with near-degenerate l states.

In this paper we present the results of measurements of $H(n=2)$ angular momentum coherences produced by collisions of protons with helium at projectile velocities faster than the orbital velocity of the helium-target electron. Because of the difficulties associated with atomic-hydrogen sources, there are as yet no measurements of angular momentum coherences for the simplest charge exchange system, protons on hydrogen atoms. For the next simplest system, protons on helium, there are only a few measurements. Zero-field quantum beats from s-d coherences have been observed in the $n=4$ manifold by Dehaes and Singer[5] but background uncertainties prevented the data from yielding relative cross sections and values for the coherences are not given. Polarization measurements of optical signals emitted from within a cell as a function of electric fields applied within the cell have produced data on coherences between s, p, and d states in the $n=3$ manifold.[6] Fitting difficulties associated with the large number of density-matrix parameters, 14 in that experiment, are presently being explored;[10] the authors noted that many unphysical parameters resulted from the original fits to the measurement. In a previous measurement of s-p coherences in the $n=2$ manifold,[4] cross sections and coherence elements were not presented, and later comparison with theory[11] required an integration of the evolution with time-dependent perturbations to account for the effects of the rapidly rising applied electric field on the evolving charge distribution as the hydrogen atoms emerged from the shielded target cell. The principal advantage of the study of coherent excitation in the $n=2$ manifold is the smaller number (five) of independent density-matrix elements. On the other hand, it requires photon detection in the uv.

ECK'S METHOD

The ensemble of final states produced in a collision is usually described by the density operator ρ for the collision process studied.[12] A choice of basis states u_i leads to a particular density-matrix representation; $\sigma_{ab}=\langle u_a|\rho|u_b\rangle$. In our experiment the scattering angle of the projectile is not observed and this imposes an axial symmetry on the density operator. Because of the short interaction times, the capture process is essentially spin independent. It should also not be significantly influenced by the weak external fields applied to perform the measurements. The initial density matrix can therefore be represented as a direct product of the electron and nuclear spin-state density matrices with the orbital-angular-momentum-state density matrix with only the last having a possible nonstatistical distribution.

Because of the symmetries outlined in the paragraph above, the $n=2$ density matrix is parametrized by only five parameters. Taking the quantization axis along the beam direction we can have nonzero diagonal elements (cross sections) σ_{lm} for σ_s, σ_{p_0}, σ_{p_1} ($\sigma_{p_{\pm 1}}$ must be equal from axial symmetry), and the complex off-diagonal coherence matrix element σ_{sp_0}. (The magnetic subscript 0 is dropped in the following.) Because only relative intensity measurements were made, we normalize the density matrix to unit trace, reducing the number of parameters that we can extract from our data to four. The normalized diagonal density-matrix elements are conveniently parametrized by the relative angular momentum cross section

$$\frac{\sigma_p}{\sigma_s}=\frac{\sigma_{p_0}+2\sigma_{p_1}}{\sigma_s}$$

and the alignment parameter A_{20},

$$A_{20}=\frac{\sigma_{p_1}-\sigma_{p_0}}{\sigma_{p_0}+2\sigma_{p_1}}\ .$$

Experimental investigations of σ_p/σ_s and A_{20} as a function of projectile velocity v have become available recently.[1,2] In the following we focus on the determination of the coherence density element σ_{sp}. This excitation parameter is not directly accessible in the field-free Lyman-α emission. We therefore employ Eck's method.[13]

The capture process is dominated by the internal fields of the projectile and target ($\approx 10^9$ V/cm) and occurs on a time scale of the order 10^{-17} s. The preparation of the excited states is thus effectively instantaneous on the time scale for their evolution and decay $\approx 10^{-9}$ s. The applied electric fields of the order 10^2 V/cm have negligible influence on the state preparation but are needed to couple σ_{sp} into the Ly-α emission. Measurements of the Ly-α intensity are made versus the time between production of the excited states and detection of their decay in electric fields F applied alternately parallel and antiparallel to the beam direction. The theoretical description of the intensity pattern contains terms arising from a nonzero σ_{sp} matrix element and terms arising from diagonal elements of the density matrix. Experimental separation of these terms is facilitated by their dependence on the field direction. The latter are independent of the applied field direction, while the former change sign upon field reversal. The sum signal $I^{\rm inc}=I(+F)+I(-F)$ thus depends only on the diagonal elements, and the difference signal $I^{\rm coh}=I(+F)-I(-F)$ depends only on σ_{sp}. In contrast to time-integral measurements,[6-8] a determination of both $\mathrm{Re}\sigma_{sp}$ and $\mathrm{Im}\sigma_{sp}$ becomes possible in a time-differential measurement without a measurement and analysis of the circular polarization of the Ly-α radiation.

In a fast beam of velocity v, time resolution is achieved by spatially localizing the target and detecting the decays from a small slice of the beam at fixed distances z from the target. Time is then related to the distance by $t=z/v$. Interference among the decays of coherently excited substates of the $n=2$ manifold leads to intensity modulations (quantum beats). The beats are observed as a spatially modulated intensity pattern in the excited beam downstream of the helium target (see Fig. 1). The spatial separation of the beat maxima is $2\pi v/\omega$. The frequency of the beats seen in Fig. 1 is approximately the perturbed Lamb-shift splitting between the Stark-shifted $2p_{1/2}$ and $2s_{1/2}$ states. We note that the signal contains additional beat frequencies. Included in the present analysis are the small hyperfine splittings which lead to low-amplitude long-wavelength modulations which have only been clearly observed in measurements with high statistics, such as obtained in beam-foil investigations.[14] Beats involving the perturbed $2p_{3/2}$ state cannot be observed because the large fine-structure splittings involved, $\approx 10\times$ the Lamb splitting, lead to short-wavelength beats which are averaged out by the finite experimental resolution.

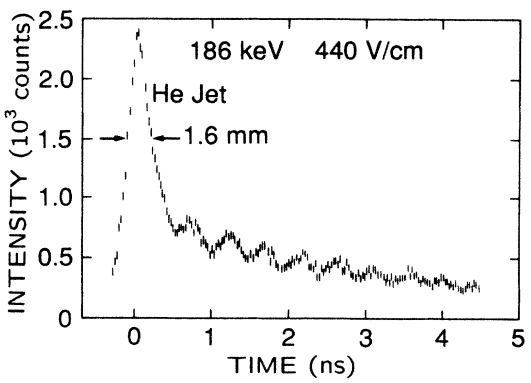

FIG. 1. Example of raw data for 186-keV proton energy in a field of 440 V/cm. The quantum beats can be seen following an emission peak from helium excited by the incident proton beam.

In the data analysis, the fitting function used is that of Burgdörfer's perturbational treatment of the evolution of the $n=2$ manifold in an external electric field including first-order corrections due to the $2p_{3/2}$ coupling, the linewidth, and the hyperfine structure.[11] The fast beats due to the $2p_{3/2}$ state are averaged over. Modifications to take into account experimental effects of background and spatial averaging are discussed in the data-analysis sections. Even for moderate field strengths $F\approx 450$ V/cm, the perturbational treatment of the evolution $I(t)$ agrees with a numerical solution to the eigenvalue problem of the 16 hyperfine levels to within a few percent.[11] The following expressions serve only as an aid to data interpretation; they have been simplified from those used in the data analysis by neglecting hyperfine corrections and terms of order $V/\omega_{\rm FS}$ and Γ/ω and are expressed in terms of parameters used in the fit:

$$I^{\rm coh}=I_0\sin 2\theta\left(1+\frac{\sigma_p}{\sigma_s}\right)[\mathrm{Re}\sigma_{sp}(\cos^2\theta\, e^{-\Gamma_1 t}-\sin^2\theta\, e^{-\Gamma_2 t}+\cos 2\theta\, e^{-\Gamma t}\cos\omega t)-\mathrm{Im}\sigma_{sp}e^{-\Gamma t}\sin\omega t]\ ,$$

$$I^{\text{inc}}=I_0\frac{1}{\sqrt{3}}\left[\frac{\sigma_p}{\sigma_s}(2-\tfrac{1}{2}A_{20})e^{-\Gamma_p t}+\left[\frac{\sigma_p}{\sigma_s}\cos^4\theta+3\sin^2\theta\cos^2\theta\right]e^{-\Gamma_1 t}\right.$$
$$\left.+\left[\frac{\sigma_p}{\sigma_s}\sin^4\theta+3\sin^2\theta\cos^2\theta\right]e^{-\Gamma_2 t}+\left[\frac{\sigma_p}{\sigma_s}-3\right]2\sin^2\theta\cos^2\theta\cos\omega t\, e^{-\Gamma t}\right] .$$

The Stark splitting is $\omega=(\omega_L^2+4V^2)^{1/2}$, where the interaction strength $V=F\langle p_{1/2}\,|\,z\,|\,s_{1/2}\rangle$, with the field strength F in a.u. and ω_L is the Lamb-shift splitting. The mixing angle in the $p_{1/2}$-$s_{1/2}$ subspace is defined through $\sin\theta\cos\theta=V/\omega$. The field-modified damping constants are given by $\Gamma=\Gamma_p/2$ and $\Gamma_{1,2}=\Gamma(1\pm\omega_L/\omega)$, and Γ_p is the field-free $2p$ decay rate. The amplitude and phase of the Stark beats in the difference signal I^{coh} allows the direct determination of the real and imaginary parts of σ_{sp}.

EXPERIMENT

The apparatus used is shown in Fig. 2. A 1-mm proton beam collimated to 6 mrad enters a 2.5-cm quench-field region. In this region, the metastable $2s$ component of the beam produced by charge exchange with background gas in the beam line is eliminated. To minimize the effects arising from electrons, a shielded field-free aperture-skimmer arrangement is used at the entrance of the quench plates and the apertures in the downstream plates are made large enough to ensure the main beam does not strike them directly. Following the quench field is the helium-jet target and the analyzer field. The quench field and analyzer field are produced by a series of 18×18-mm square plates spaced 12.5 and 6.3 mm apart and biased by a series of 500 and 250 kΩ resistors, respectively. The resistors were hand picked for uniformity to less than 1%. V-shaped cutouts around 4.5-mm holes in the analyzer-field plates allow uninterrupted viewing of the light emissions at right angles to the beam direction. Numerical solutions of Laplace's equation indicate that within the beam diameter the analyzer-field inhomogeneities are no larger than 5%. The voltages applied to the ends of the resistor chain were of opposite sign and adjusted so that the voltage at the helium jet was near ground potential. The analyzer and quench fields were simultaneously reversed at the end of a scan by reversing the polarity of the voltages applied to the resistor chain. The beam is finally collected in a Faraday cup for signal normalization.

The helium-jet target is produced by a conductive microcapillary array (10-μm-diam channels in a hexagonal pattern with a 15-μm spacing) mounted to a hypodermic needle of inside diameter 0.35 mm. The needle protrudes midway between the first two field plates 1 mm from the beam and is also biased by the resistor chain to minimize field inhomogeneities. Small changes in its biasing had no observable effect on the data. The needle positioning could be adjusted to maximize the beam-jet interaction, or to move the needle several millimeters to the side of the beam.

The optical system is mounted at right angles to the beam direction on an XYZ manipulator. It consists of a LiF collector lens which focuses the light emitted into a cone of half-angle 11° from a small section of the beam onto a Hamamatsu model R1259 uv-sensitive photomultiplier tube. To check the focusing, a circular aperture defining a viewing region 0.5 mm in diameter was used and the optics were scanned vertically across the proton

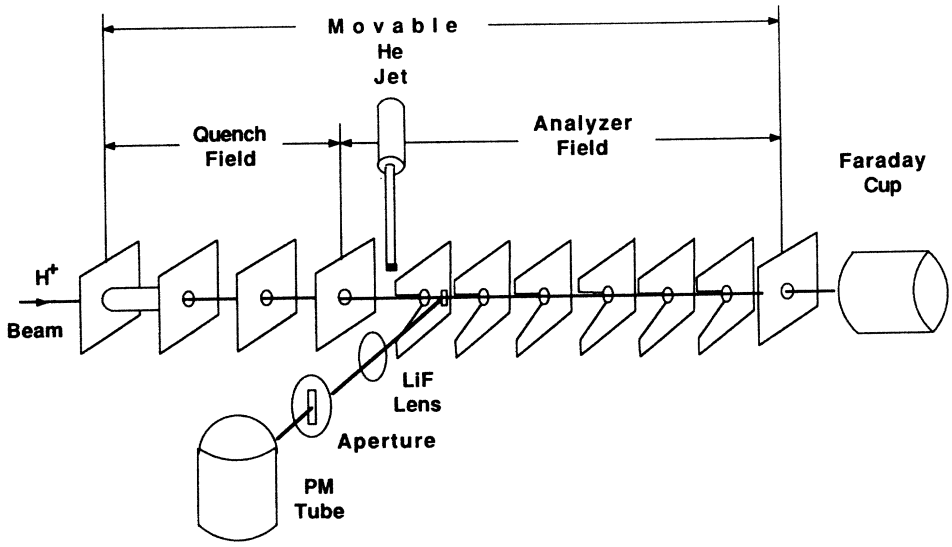

FIG. 2. Schematic of experimental apparatus. The field plates and He target jet move in front of a fixed viewing region.

beam at a fixed distance 1 cm downstream from the He target. At optimum focus, a symmetric profile of about 1.5 mm full width at half maximum (FWHM) was observed—consistent with the beam profile as defined by the apertures. The data were taken with a slit aperture which imaged to a 0.5×1.5-mm^2 rectangle to collect fully across the beam diameter without increasing the length of beam viewed.

The target and field plates are mounted on a stepper-motor-controlled linear stage, aligned to the beam direction. This stage is moved upstream with a fixed optical positioning to produce spectra of intensity versus distance (time) from the interaction region as illustrated in Fig. 1. The spectrum shows a strong peak resulting from emissions of beam-excited helium followed by the quantum beats. The FWHM of the helium peak is about 1.6 mm. This width agrees with that obtained by viewing the Ly-α emissions downstream of the target as the needle is scanned across the proton beam.

To check single-collision conditions, the intensity was measured as the pressure behind the needle was varied. A linear relation was verified in the range of pressures used in the experiment. The target-chamber pressure was $\approx2\times10^{-6}$ Torr. The effectiveness of the quench field was demonstrated by dumping helium directly into the chamber to a pressure of 2×10^{-5} Torr. Without the quench field, beats from the metastable $2s_{1/2}$ states were clearly observable and were reduced by $\approx90\%$ when the quench field was applied. With the normal gas flow used in the experiment, applied by positioning the He jet about 3 mm off to the side of the beam, and with the quench field, a slowly varying, nonbeating background was observed.

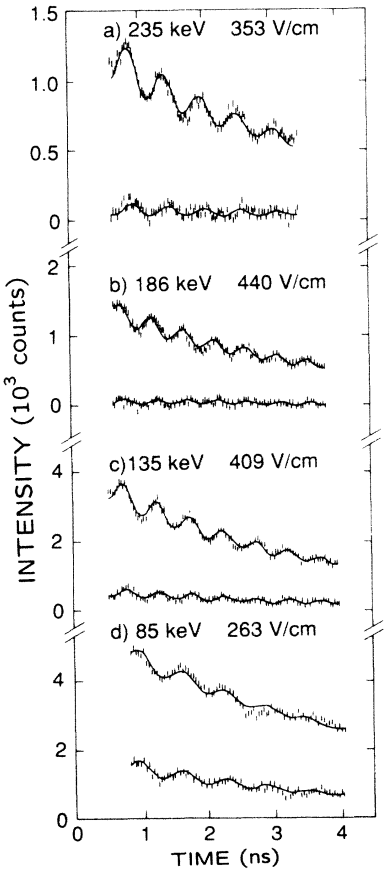

FIG. 3. Data and fitted function for 135–235-keV collision energy. The upper curves are $I^{\rm inc}$ and the lower curves are $I^{\rm coh}$.

DATA ANALYSIS

Data were taken at 85- 135- 186- and 235-keV collision energy. Intensity distributions were measured at three different field strengths from 263 to 440 V/cm, except for the 85-keV data which were measured at only two field strengths 263 and 351 V/cm. As the density matrix should be independent of the field strength, this provides a check on the consistency of the data. At each energy and field strength, the coherent and incoherent signals were simultaneously fitted to the theoretical expressions of Ref. 11 as follows. Data were analyzed starting at positions well away from the helium peak as illustrated in Fig. 3. Not including the field-dependent frequencies and lifetimes contained in the expressions, which were fixed at their theoretical values, the fit contained ten parameters. The density matrix accounts for five parameters including the normalization factor. Backgrounds for the coherent and incoherent signal were satisfactorily modeled using different amplitudes but a single-exponential damping constant. A beat-reduction factor multiplying the oscillatory terms in the fitting function was used to incorporate the effects of experimental averaging (described in the following). The final parameter is the effective position of the excitation or channel where the evolution of the initial density matrix formed in the collision is assumed to begin (the $t=0$ point).

The helium peak spatial position and width, measured by the emissions as the jet passes through the viewing region, was consistent from run to run. The observed width should have a contribution from the averaging due to the optics in addition to the gas density profile within the jet. With the plausible assumption that the helium excitation within the jet mimics the excited hydrogen production, one can obtain the $t=0$ point from the position of the peak and the effects of spatial averaging can be obtained by convoluting theoretical intensity patterns with observed helium peak shapes. The only intensity variations that are expected to be affected noticeably by the convolution are the quantum beats. Therefore a simpler technique eliminating the need for repeated convolutions was adopted.

Numerical convolutions of the observed helium peak shape with theoretical intensity patterns of varying beat length were virtually indistinguishable from patterns obtained by multiplying oscillatory terms in the theoretical formulas by a beat-reduction factor (BRF). The BRF depended only on the beat length. BRF's obtained from convolutions of helium peak shapes from different runs as well as from a Gaussian peak shape with 1.6 mm FWHM typically varied by ±0.07, which was taken as its uncertainty. We thus take the $t=0$ point and the BRF as known parameters of the fit (within some error limits).

We observed a large and field-dependent background. It was larger (relative to the signal) for higher collision

TABLE I. Fitting results for 135-keV protons on helium for field strength of 409 V/cm. The entries illustrate the dependence of the s-p coherence element on various assumptions about uncertain experimental or theoretical quantities.

BRF	σ_p/σ_s	A_{20}	$t=0$	norm	$\mathrm{Re}\sigma_{sp}$	$\mathrm{Im}\sigma_{sp}$	χ^2
0.24	0.10	−0.4	N	1	0.28	0.09	1.6
0.24	0.15	−0.4	N	1	0.29	0.09	1.5
0.24	0.20	−0.4	N	1	0.30	0.08	1.6
0.24	0.15	0.0	N	1	0.29	0.09	1.6
0.24	0.15	−1.0	N	1	0.31	0.09	1.5
0.17	0.15	−0.4	N	1	0.36	0.10	1.6
0.31	0.15	−0.4	N	1	0.29	0.09	1.6
0.24	0.15	−0.4	N	0.95	0.26	0.09	1.6
0.24	0.15	−0.4	N	1.05	0.32	0.09	1.6
0.24	0.15	−0.4	$-\frac{1}{2}$ch.	1	0.26	0.12	2.1
0.24	0.15	−0.4	$+\frac{1}{2}$ch.	1	0.32	0.05	2.5

energies, smaller field strengths, and for the parallel field configuration. The other measurements[4–6] mentioned in the Introduction also showed a background dependence on field direction. Clearly any future measurements should address this problem directly.

Uncertainties in the background determination, together with the functional dependence of the signal on σ_p/σ_s, A_{20}, and σ_{sp}, make a simultaneous accurate and unique determination of all of them virtually impossible. We therefore use σ_p/σ_s and A_{20} obtained from independent experimental measurements[1,2] taken without applied electric fields and from theoretical results[11,15] in the fit. The small variations in the fitted values of σ_{sp} arising from the uncertainties in the values used for σ_p/σ_s and A_{20} are included in the quoted uncertainties.

In Fig. 3 we show fits to 4 of the 11 data sets; one for each energy. The fit of Fig. 3(c) corresponds to row 2 of Table I in which we present the results of a series of fits performed on this data set. Table I gives fitted values $\mathrm{Re}\sigma_{sp}$ and $\mathrm{Im}\sigma_{sp}$ and the reduced χ^2 for the fit for different fixed values of the BRF, σ_p/σ_s, alignment, $t=0$ point, and normalization errors.

In the first three rows we illustrate the effect of varying σ_p/σ_s on the fit. The BRF has been fixed at its experimentally determined value (for this beat length) of 0.24, while σ_p/σ_s is varied between 0.1 and 0.2 which corresponds to the range of values found in the measurements of Hughes *et al.*,[1] the post-collision interaction (PCI),[11] and coupled-state calculations.[15] The constancy of the χ^2 illustrates the insensitivity of the data to σ_p/σ_s, while the coherence parameters show only modest changes. In these fits the normalization and background changed by ±4% and ±15%, respectively. Likewise, the next two lines show that the χ^2 is also nearly independent of the alignment assumed. The experimentally determined alignment of Hippler *et al.*[2] is approximately −0.4 in our energy range. The next two lines illustrate the effects of changing the BRF ±0.07 from its nominal value. In the next two rows the effects of a 5% error in normalization between the two field directions is examined. The column labeled norm gives the assumed normalization of the antiparallel field direction relative to the parallel field direction. While no systematic differences in the beam current were noticed when the field was reversed, and under ideal conditions this factor should be unity, it is difficult to completely rule out such a normalization error entirely, as focusing in the fringing fields of the field plates may have an effect especially at the lower beam energies. Also shown are the effects of moving the $t=0$ point $\pm\frac{1}{2}$ channel from its experimentally determined position.

RESULTS AND DISCUSSION

Table II shows the results for the real and imaginary parts of σ_{sp} for each energy and field strength. Changes in σ_{sp} were found as in Table I for variations in the BRF of ±0.07 from its nominal value, the $t=0$ position by $\pm\frac{1}{2}$ channel (±0.08 mm), σ_p/σ_s from 0.1 to 0.2, the alignment from 0 to −1, and the relative normalization from 0.95 to 1.05. As these are 2-σ variations in the fixed parameters, the resulting nearly symmetric changes in σ_{sp} were halved and added in quadrature with the counting statistics error to arrive at the final 1-σ errors given in parentheses in the table. Checks were also made that changes in σ_{sp} resulting from variations in any two fixed parameters were well described keeping only the first derivatives as established from the procedure above.

The sample of the fitted 85-keV data shown in Fig. 3(d) has a beat length of just about 2 mm and there is a severe loss of information associated with the small BRF that results (0.15). Also the accelerator performance at this energy was poor, and while beam currents were small ($\approx$25 nA), fluctuations were large. Because the data at this energy is of questionable reliability, we disregard it in the following discussion.

Several classifications of angular momentum coherences in terms of expectation values of multipoles built from various operators have been proposed (Ref. 7, and references therein). In Fig. 4 we present the results for the s-p coherence together with recent theoretical re-

TABLE II. Summary of experimental results.

Energy (keV)	v (a.u.)	Field (V/cm)	$\mathrm{Re}\sigma_{sp}$	$\mathrm{Im}\sigma_{sp}$	χ^2
235	3.06	264	0.12(0.04)	0.14(0.04)	2.1
		353	0.19(0.04)	0.11(0.03)	1.4
		406	0.20(0.05)	0.13(0.04)	1.6
	Average		0.17(0.04)	0.13(0.04)	
186	2.73	296	0.22(0.04)	0.17(0.04)	1.3
		357	0.17(0.04)	0.12(0.03)	1.8
		440	0.16(0.05)	0.15(0.05)	1.9
	Average		0.18(0.04)	0.15(0.04)	
135	2.32	267	0.11(0.03)	0.13(0.02)	2.8
		355	0.19(0.04)	0.12(0.04)	2.6
		409	0.29(0.05)	0.09(0.04)	1.5
	Average		0.20(0.04)	0.12(0.04)	

sults[16,17] in terms of the expectation values of the normalized Runge-Lenz vector $\mathbf{a}=(n/Z_p)\mathbf{A}$ and the angular momentum vector $\mathbf{L}$,

$$\langle \mathbf{a} \rangle_z = 2\,\mathrm{Re}\sigma_{sp} ,$$

$$\langle \mathbf{L}\times\mathbf{a} \rangle_z = 2\,\mathrm{Im}\sigma_{sp} ,$$

where

$$\mathbf{A}=\tfrac{1}{2}(\mathbf{p}\times\mathbf{L}-\mathbf{L}\times\mathbf{p})-Z_p\hat{\mathbf{r}} .$$

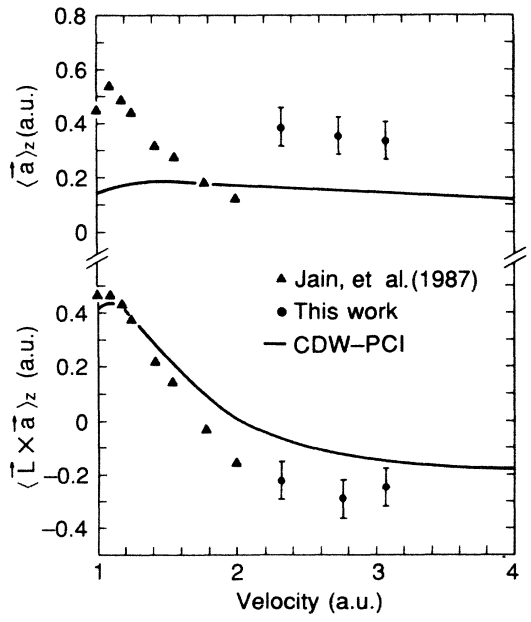

FIG. 4. Theoretical and experimental $n=2$ coherence parameters $\langle \mathbf{a} \rangle_z$ and $\langle \mathbf{L}\times\mathbf{a} \rangle_z$. +, coupled-states calculation (Ref. 17); –, CDW-PCI (Ref. 16); ●, present experimental data.

The expectation value of a_z describes the forward-backward asymmetry of the charge cloud while $\mathbf{L}\times\mathbf{a}$ gives within a classical picture the direction of the orbital velocity at perihelion.

Nonvanishing values of $\langle \mathbf{a} \rangle_z$ are a direct measure of higher-order Born effects since the first Born approximation (OBK approximation) gives[3,18] $\langle \mathbf{a} \rangle_z = 0$. The CDW-PCI approximation, which includes long-range Stark mixing effects of nearly degenerate states in the exit channel, gives $\langle \mathbf{a} \rangle_z > 0$ in agreement with the experiment indicating that the charge cloud lags behind the proton. However, the asymmetry is too low by about a factor of 2, in agreement with previous findings[18] for higher-n states and for electron capture to the continuum. This clearly indicates an incomplete representation of multiple-scattering effects in the CDW approximation. At lower velocities ($1 \le v \le 2$ a.u.) the recent coupled-channel calculation by Jain *et al.*[17] gives larger values for $\langle \mathbf{a} \rangle_z$ which, however, rapidly decrease with increasing v and fall below the CDW value near 80 keV ($v \approx 1.8$ a.u.). At these velocities the incorporation of significant contributions from continuum intermediate states in an atomic-orbital expansion with a relatively small number of channels poses a possible problem.

Turning now to the expectation value of $\langle \mathbf{L}\times\mathbf{a} \rangle_z$, we note that the CDW-PCI approximation underestimates the absolute value of the experimental data. Nevertheless, it reproduces the qualitative trend of the experimental and numerical data from the coupled-states calculations[17] which implicitly includes PCI effects surprisingly (and, in fact, fortuitously) well. The change of sign in $\langle \mathbf{L}\times\mathbf{a} \rangle_z$ in the close-coupling results near $v \approx 1.7$ a.u. is reproduced by the CDW-PCI calculation even though shifted to slightly higher v. It should be noted that a CDW calculation without inclusion of PCI effects does not display a change of sign in $\langle \mathbf{L}\times\mathbf{a} \rangle_z$ in this velocity region. Unfortunately, the quantum beat technique is not easily applicable to lower velocities because of the resulting short beat wavelengths. The change of sign could therefore not be measured. However, complementary

data by the North Carolina State group[6,8] for the $n=3$ density matrix at lower energies show positive values for $\langle \mathbf{L}\times\mathbf{a}\rangle_z$ which approach zero at the upper end of the range of collision energies (≈ 80 keV). Combining these two measurements and taking into account the theoretically predicted weak n dependence of the coherence parameters, the change of sign seems to be established. This indicates that $\langle \mathbf{L}\times\mathbf{a}\rangle_z$ provides a direct and sensitive measure for the importance of long-range intrashell Stark mixing in the exit channel.

ACKNOWLEDGMENTS

We thank A. Jain, C. D. Lin, and W. Fritsch for sending us their data prior to publication. This experiment was carried out at the Solid State Accelerator Laboratory of Oak Ridge National Laboratory. The cooperation of W. White and O. E. Schow is gratefully acknowledged. This research was supported in part by the National Science Foundation and by the U. S. Department of Energy, under Contract No. DE-AC05-84OR21400 with Martin Marietta Energy Systems, Inc.

[1]R. H. Hughes, E. D. Stokes, Song-Sik Choe, and T. J. King, Phys. Rev. A **4**, 1453 (1971); R. H. Hughes, C. A. Stigers, B. M. Doughty, and E. D. Stokes, *ibid.* **1**, 1424 (1970).

[2]R. Hippler, W. Harbich, M. Faust, H. O. Lutz, and L. J. Dubé, J. Phys. B **19**, 1507 (1986).

[3]J. Burgdörfer and L. J. Dubé, Nucl. Instrum. Methods B **10/11**, 198 (1985).

[4]I. A. Sellin, L. Liljeby, S. Mannervik, and S. Hultberg, Phys. Rev. Lett. **42**, 570 (1979); L. Liljeby, S. Mannervik, S. Hultberg, and I. A. Sellin, in *Coherence and Correlation in Atomic Collisions,* edited by H. Kleinpoppen and J. F. Williams (Plenum, New York, 1980), pp. 447–455.

[5]J. C. Dehaes and W. Singer, Phys. Lett. **75A**, 276 (1980).

[6]C. C. Havener, W. B. Westerveld, J. S. Risley, N. H. Tolk, and J. C. Tully, Phys. Rev. Lett. **48**, 926 (1982); C. C. Havener, N. Rouze, W. B. Westerveld, and J. S. Risley, Phys. Rev. A **33**, 276 (1986).

[7]J. Burdörfer, Z. Phys. A **309**, 285 (1983).

[8]P. Van der Straten, R. Morgenstern, Comments At. Mol. Phys. **XVII**, 243 (1986).

[9]Y. Yamazaki, P. D. Miller, H. F. Krause, P. L. Miller, S. Datz, I. A. Sellin, and N. Stolterfoht, Phys. Rev. Lett. **57**, 992 (1986).

[10]J. R. Ashburn, R. A. Cline, P. J. M. Van der Burgt, W. B. Westerveld, and J. S. Risley, Bull. Am. Phys. Soc. **32**, 490 (1987); *Abstracts of the Fifteenth International Conference on the Physics of Electronic and Atomic Collisions, Brighton, United Kingdom, 1987,* edited by J. Geddes, H. B. Gilbody, A. E. Kingston, C. J. Latimer, and H. J. R. Walters (Queens University, Belfast, 1987), p. 490.

[11]J. Burgdörfer, Phys. Rev. A **24**, 1756 (1981); Ph.D. thesis, Freie Universität Berlin, 1981.

[12]U. Fano, Revs. Mod. Phys. **29**, 74 (1957).

[13]T. G. Eck, Phys. Rev. Lett. **31**, 270 (1973).

[14]H. J. Andrä, Phys. Scr. **9**, 257 (1973).

[15]T. G. Winter and C. C. Lin, Phys. Rev. A **5**, 2141 (1974).

[16]J. Burgdörfer, Phys. Rev. A **33**, 1578 (1986).

[17]A. Jain, C. D. Lin, and W. Fritsch, Phys. Rev. A **36**, 2041 (1987).

[18]J. Burgdörfer and L. J. Dubé (unpublished).